

Ligand Conformational Bias Drives Enantioselective Modification of a Surface-Exposed Lysine on Hsp90

Adolfo Cuesta, Xiaobo Wan, Alma L. Burlingame, and Jack Taunton*



Cite This: *J. Am. Chem. Soc.* 2020, 142, 3392–3400



Read Online

ACCESS |



Metrics & More

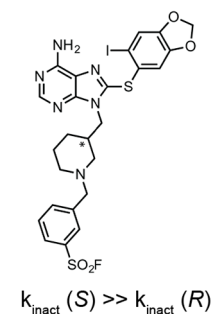
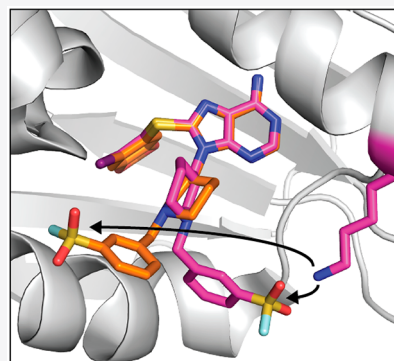


Article Recommendations



Supporting Information

ABSTRACT: Targeted covalent modification of surface-exposed lysines is challenging due to their low intrinsic reactivity and high prevalence throughout the proteome. Strategies for optimizing the rate of covalent bond formation by a reversibly bound inhibitor (k_{inact}) typically involve increasing the reactivity of the electrophile, which increases the risk of off-target modification. Here, we employ an alternative approach for increasing k_{inact} of a lysine-targeted covalent Hsp90 inhibitor, independent of the reversible binding affinity (K_i) or the intrinsic electrophilicity. Starting with a noncovalent ligand, we appended a chiral, conformationally constrained linker, which orients an arylsulfonyl fluoride to react rapidly and enantioselectively with Lys58 on the surface of Hsp90. Biochemical experiments and high-resolution crystal structures of covalent and noncovalent ligand/Hsp90 complexes provide mechanistic insights into the role of ligand conformation in the observed enantioselectivity. Finally, we demonstrate selective covalent targeting of cellular Hsp90, which results in a prolonged heat shock response despite concomitant degradation of the covalent ligand/Hsp90 complex. Our work highlights the potential of engineering ligand conformational constraints to dramatically accelerate covalent modification of a distal, poorly nucleophilic lysine on the surface of a protein target.



INTRODUCTION

Covalent inhibitors have broad utility as drugs, cell biological tools, and chemoproteomic probes. Irreversible covalent modification results in drug-target residence times that match the lifetime of the targeted protein, often independent of the drug clearance rate.^{1,2} Additionally, covalent inhibitors can discriminate between closely related paralogs by reacting with a nonconserved nucleophilic amino acid within or near the ligand binding site.^{3–8} Selective modification of the intended nucleophile is determined by a two-step reaction mechanism in which reversible binding of the ligand precedes covalent modification. Both the reversible binding affinity and the rate of covalent bond formation within the initially formed noncovalent complex (k_{inact}) contribute to the potency of covalent inhibitors.⁹ An obvious way to increase k_{inact} is to augment the intrinsic reactivity of the electrophile. A downside of this approach is that it increases the likelihood of undesired off-target reactions. Optimization of covalent inhibitors therefore relies primarily on maximizing the reversible binding affinity of the noncovalent recognition element.^{10,11} To date, the design of rapid-acting, highly selective covalent ligands has focused on cysteine, in part because its high intrinsic reactivity permits the use of relatively unreactive electrophiles (e.g., acrylamides).^{12–14} Cysteine is one of the least prevalent amino acids in the proteome, however, and many ligand binding sites lack a proximal cysteine.

Lysine is more prevalent than cysteine, and its side-chain amine is therefore a potentially attractive target for covalent inhibitor design.^{15,16} Nevertheless, rapid and selective covalent modification of lysine is challenging. First, the side-chain amine is mostly protonated at physiological pH and has attenuated reactivity. Second, the butylamine side chain has many conformational degrees of freedom. This enhanced flexibility results in an entropic cost to covalent capture, potentially complicating the design of inhibitors with high k_{inact} . Third, the high prevalence of lysine in the proteome increases the probability of off-target reactions. All of these challenges are exacerbated when attempting to target a surface-exposed lysine.

Arylsulfonyl fluorides, which are weakly reactive toward water and simple amines at physiological pH, have been employed as covalent lysine-targeted inhibitors of protein kinases and stabilizers of mutant transthyretin.^{17–19} However, in these proteins, the targeted lysines are in hydrophobic ligand binding sites, form specific hydrogen bonds with proximal amino acid side chains, and likely have perturbed pK_a s.^{18,20}

Received: September 7, 2019

Published: February 3, 2020



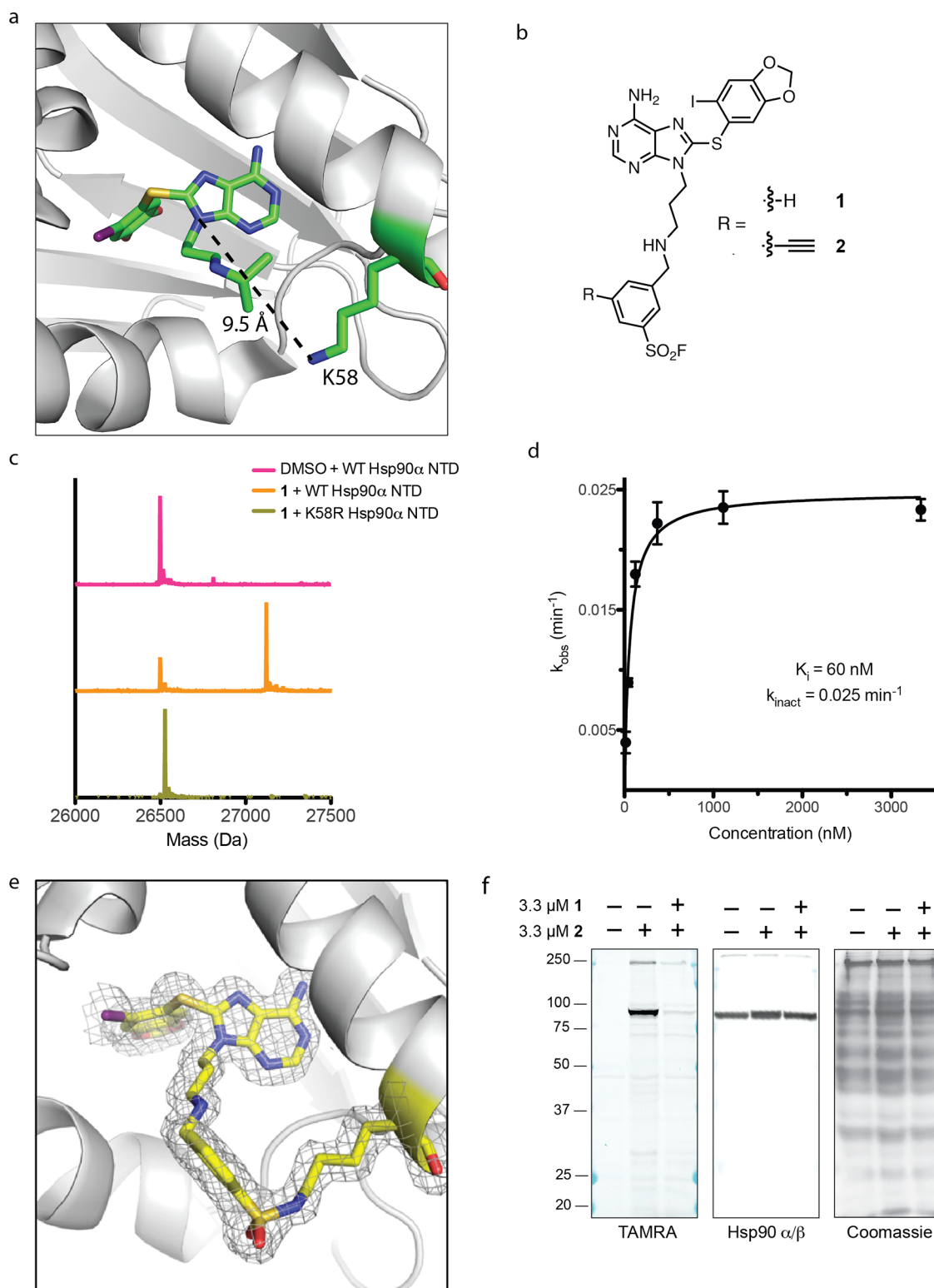


Figure 1. Design of lysine-targeted arylsulfonyl fluoride inhibitors of Hsp90. (a) Lys58 is within 9.5 Å of the purine moiety of PU-H71 (PDB code: 2FWZ). (b) Arylsulfonyl fluorides **1** and **2**. (c) Intact-protein MS analysis of WT and K58R Hsp90 NTD treated with **1** (10 μM, 1 h, 37 °C). (d) Kinetic analysis (k_{obs} , min^{-1}) of Hsp90 NTD covalent modification in the presence of increasing concentrations of **1**. (e) Crystal structure of **1**/Hsp90 (1.8-Å resolution). Electron density ($2F_o - F_c$) is shown at a contour level of 1σ . (f) Skbr3 cells were treated with probe **2** (90 min), followed by cell lysis and TAMRA-azide conjugation. Samples were analyzed by in-gel fluorescence and Western blotting for Hsp90.

Whether arylsulfonyl fluorides are sufficiently reactive to rapidly modify a solvated lysine on the surface of a protein remains underexplored.^{21,22} Here, we report the design of arylsulfonyl fluorides that selectively target Lys58 on the

surface of the heat shock protein, Hsp90, a critical regulator of cellular proteostasis.²³ Although cyanoethyl acylsulfonamide probes were recently developed to modify Hsp90 on Lys58, the structural and mechanistic details of this reaction were not

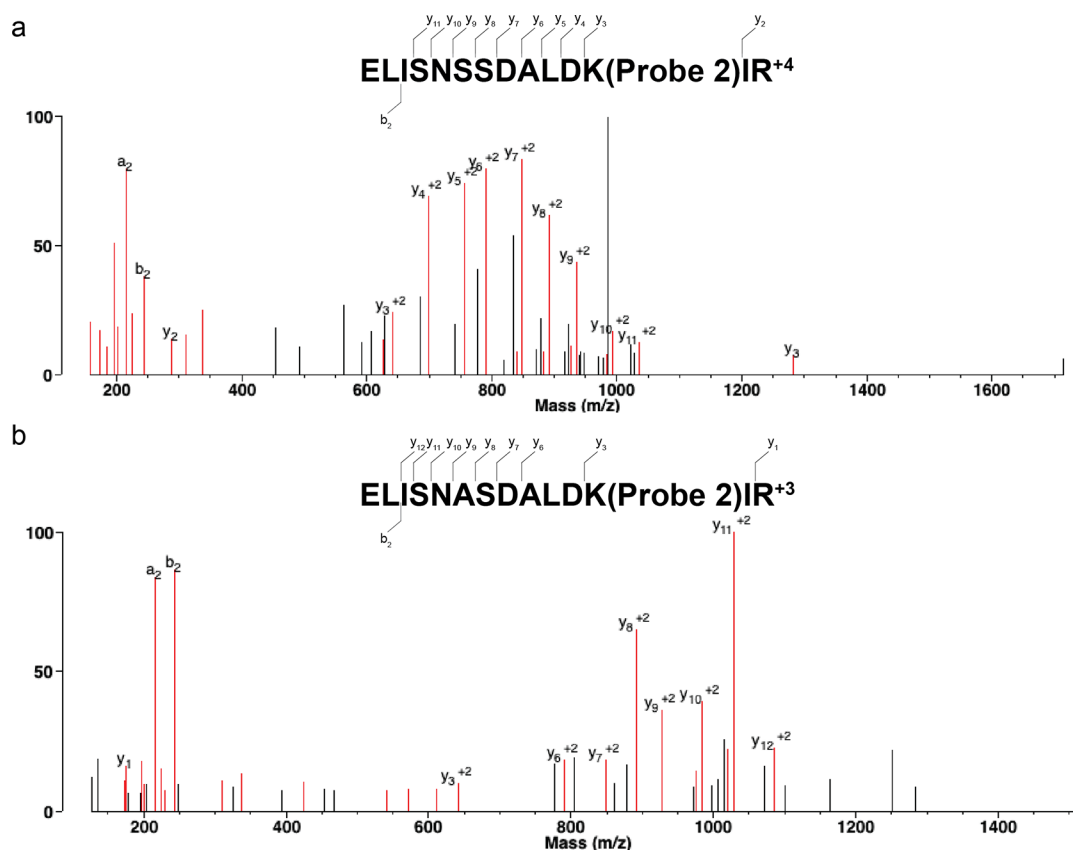


Figure 2. MS/MS spectra of probe 2-labeled peptides derived from Hsp90 α (a) and Hsp90 β /Grp94 (b). Cells were treated with probe 2, and covalently modified proteins were enriched with streptavidin-agarose beads after click conjugation with a hydrazine-cleavable biotin-azide reagent. After on-bead trypsinization and extensive washing, probe-modified peptides were eluted via hydrazine cleavage and analyzed by LC-MS/MS (see [Supporting Information](#) for details). Assigned MS2 fragments are indicated in red.

explored.²⁴ By contrast, our mechanistic studies reveal how chiral conformational constraints in the ligand enantioselectively increase the rate of covalent bond formation, independent of the ligand's reversible binding affinity.

RESULTS AND DISCUSSION

We used the crystal structure of the Hsp90 N-terminal ATPase domain (NTD) bound to the reversible inhibitor, PU-H71,²⁵ as a starting point to develop electrophilic inhibitors that target Lys58. This surface-exposed lysine lies outside the ATP pocket, 10 Å from the purine core of PU-H71 (Figure 1a). Our covalent Hsp90 inhibitors are based on a modular design, including (1) a noncovalent recognition scaffold based on PU-H71, (2) an arylsulfonyl fluoride electrophile, and most critically, (3) a variable linker to orient the arylsulfonyl fluoride toward Lys58. On the basis of the inherent flexibility of both the propylamine linker in PU-H71 and the side chain of Lys58, we reasoned that an arylsulfonyl fluoride would be tolerated as a replacement for the isopropyl group, leading to the design of arylsulfonyl fluorides **1** and **2** (Figure 1b). Treatment of recombinant Hsp90 NTD (N-terminal ATPase domain) with a saturating concentration of arylsulfonyl fluoride **1** (10 μ M, 1 h) resulted in the formation of a 1:1 covalent adduct, as revealed by mass spectrometry (Figure 1c). Kinetic analysis using this assay revealed $k_{\text{inact}} \sim 0.025 \text{ min}^{-1}$ ($t_{1/2} \sim 30 \text{ min}$) and $K_i \sim 60 \text{ nM}$ (Figure 1d and S1), with K_i being similar to the published equilibrium dissociation constant of PU-H71.²⁶ Mutation of Lys58 to arginine abrogated covalent modification, despite the presence of 16 other lysines in the Hsp90 NTD (Figure 1c).

To reveal the binding mode of arylsulfonyl fluoride **1** after modification of Hsp90 NTD, we crystallized the covalent complex and determined the structure at a resolution of 1.8 Å. The purine thioether of **1** superimposes perfectly with the previously determined cocrystal structure of PU-H71. In contrast to PU-H71, the propylamine linker of **1** adopts a fully extended conformation, whereas the conformation of the Lys58 side chain is slightly kinked. Continuous electron density between Lys58 and the sulfonyl group of **1** provided unambiguous evidence for a covalent bond (Figure 1e).

We next characterized the selectivity of arylsulfonyl fluoride **1** in cells. We synthesized alkyne **2** as a clickable version of **1** suitable for cellular target engagement experiments. Skbr3 cells were treated with **2** (3.3 μ M, 90 min) and probe-labeled proteins were visualized by in-gel fluorescence after copper-catalyzed conjugation of TAMRA-azide (TAMRA = tetramethylrhodamine). This revealed a prominent 90-kDa band, which was strongly competed by pretreating cells with an equivalent concentration of **1** (Figure 1f).

To identify the cellular protein targets and modification sites of probe **2** in an unbiased manner, we used a hydrazine-cleavable biotin-azide in the click conjugation step, followed by neutravidin-agarose enrichment and on-bead trypsinization (3 biological replicates). Mass spectrometry analysis of the on-bead tryptic digest revealed the cytosolic Hsp90 paralogs, Hsp90 α and Hsp90 β (HSP90AA1 and HSP90AB1), as the proteins most strongly competed by **1** (\log_2 ratio ~ 3.5 , Supplemental Table S1). Known Hsp90 cochaperones (e.g., Cdc37) were also identified in this fraction (Supplemental

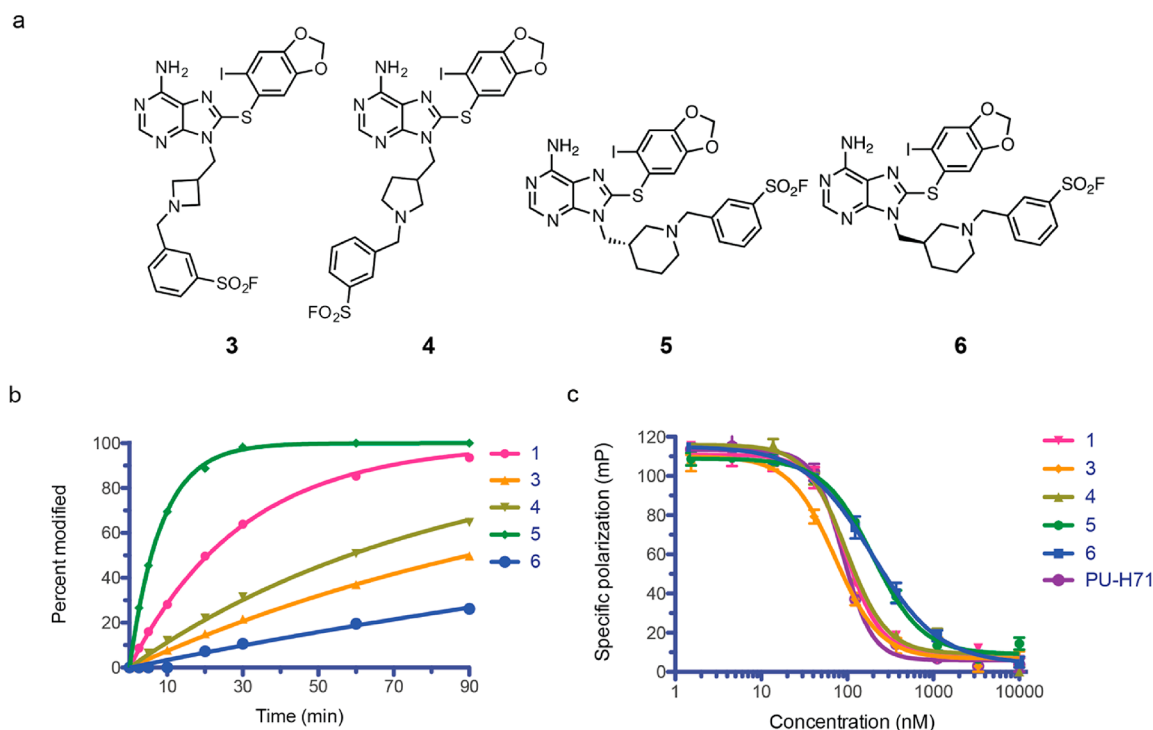


Figure 3. Linker conformational constraints dramatically affect k_{inact} . (a) Compounds 3–6. (b) Hsp90 α NTD was treated with the indicated compounds at 10 μM , and the extent of covalent modification over time was measured by LC-MS. (c) Equilibrium binding of 1, 3–6, and PU-H71 to K58R Hsp90 α NTD (30 nM) was measured by competition with FITC-geldanamycin (5 nM) in a fluorescence polarization assay. For $t_{1/2}$ and IC_{50} values derived from (b) and (c), see Table S3.

Table S1). Hydrazine-mediated cleavage of the immobilized biotin linker, followed by mass spectrometry analysis, led to the identification of only two probe-modified peptides in all three biological replicates. One peptide derives from Hsp90 α (aa 47–60), whereas the amino acid sequence of the second peptide matches both Hsp90 β (aa 42–55) and the related paralog Grp94 (aa 103–116) (Figure 2a,b). The MS2 spectra provided unambiguous evidence for covalent modification of the intended lysine (Lys58 based on Hsp90 α numbering). Because Hsp90 α/β were competed to a much greater extent than Grp94 (~8-fold vs ~2-fold, Figure S2), it is likely that arylsulfonyl fluoride 1 potently engages Hsp90 α and Hsp90 β in cells, whereas it weakly engages Grp94. In conclusion, arylsulfonyl fluorides 1 and 2 demonstrate significant Hsp90 occupancy and appear to selectively modify Lys58 in cells.

Given that the rate of Hsp90 modification by arylsulfonyl fluoride 1 is relatively slow ($t_{1/2} \sim 30$ min, Figure 1d), a key question concerns whether the sulfonyl fluoride is optimally positioned to facilitate nucleophilic attack by Lys58 within the context of the initial reversible complex. In an attempt to reduce the entropic penalty of adopting a Lys58-reactive conformation, we constrained the propylamine linker within a 4-, 5-, or 6-membered ring to give azetidine 3, pyrrolidine 4 (synthesized as a racemic mixture) and the enantiomerically pure piperidines 5 and 6 (Figure 3a). We measured Hsp90 modification rates at a compound concentration of 10 μM , i.e., 250-fold higher than the K_d of PU-H71.²⁶ Assuming the different linkers do not substantially alter the reversible binding affinity, this simple measurement should reveal the relative rates of covalent bond formation between Lys58 and reversibly bound 1 and 3–6 (i.e., relative k_{inact} values). Strikingly, sulfonyl fluoride 5, which has the (*S*)-methylpiperidine linker, exhibited the fastest modification rate ($t_{1/2} \sim 5$ min), while its

enantiomer 6 was the slowest compound tested ($t_{1/2} \sim 200$ min) (Figure 3b, Table S3).

To confirm that the observed modification rates primarily reflect differences in k_{inact} and not the reversible binding affinity, we determined the relative binding affinities of 1 and 3–6 using the K58R mutant of Hsp90 NTD, which is resistant to covalent modification. Using an established fluorescence polarization assay with FITC-geldanamycin as the fluorescent ligand,²⁷ we found that compounds 1 and 3–6 compete with FITC-geldanamycin for binding to Hsp90 with similar IC_{50} values (Figure 3c, Table S3). These data suggest that compounds 1 and 3–6 bind Hsp90 with similar affinities and that the observed modification rates at 10 μM are maximal, i.e., they correspond to k_{inact} . We also measured the concentration- and time-dependent modification of Hsp90 by enantiomers 5 and 6 (Figure S3 and S4), which revealed k_{inact} values of 0.13 min^{-1} and 0.004 min^{-1} , respectively (32-fold), and K_i values of 164 nM and 378 nM, respectively (2.3-fold). Together, these data indicate that the increased rate of Hsp90 modification by 5 is driven primarily by k_{inact} . Given that the intrinsic reactivities of sulfonyl fluorides 5 and 6 are identical, we hypothesized that the (*S*)-methylpiperidine linker of 5, and not the (*R*)-methylpiperidine linker of 6, specifically orients the arylsulfonyl fluoride toward Lys58 on the surface of Hsp90.

We used X-ray crystallography to provide structural insights into the dramatic difference in Hsp90 modification rates exhibited by the enantiomers 5 and 6. As expected, the structure of 5 bound to Hsp90 (1.8 Å resolution) revealed continuous electron density between the sulfonyl group and Lys58, consistent with covalent bond formation (Figure 4a). We next solved the structure of the noncovalent complex of 5 bound to the K58R mutant of Hsp90 (1.65 Å resolution). Although the Arg58 side chain is disordered in this structure,

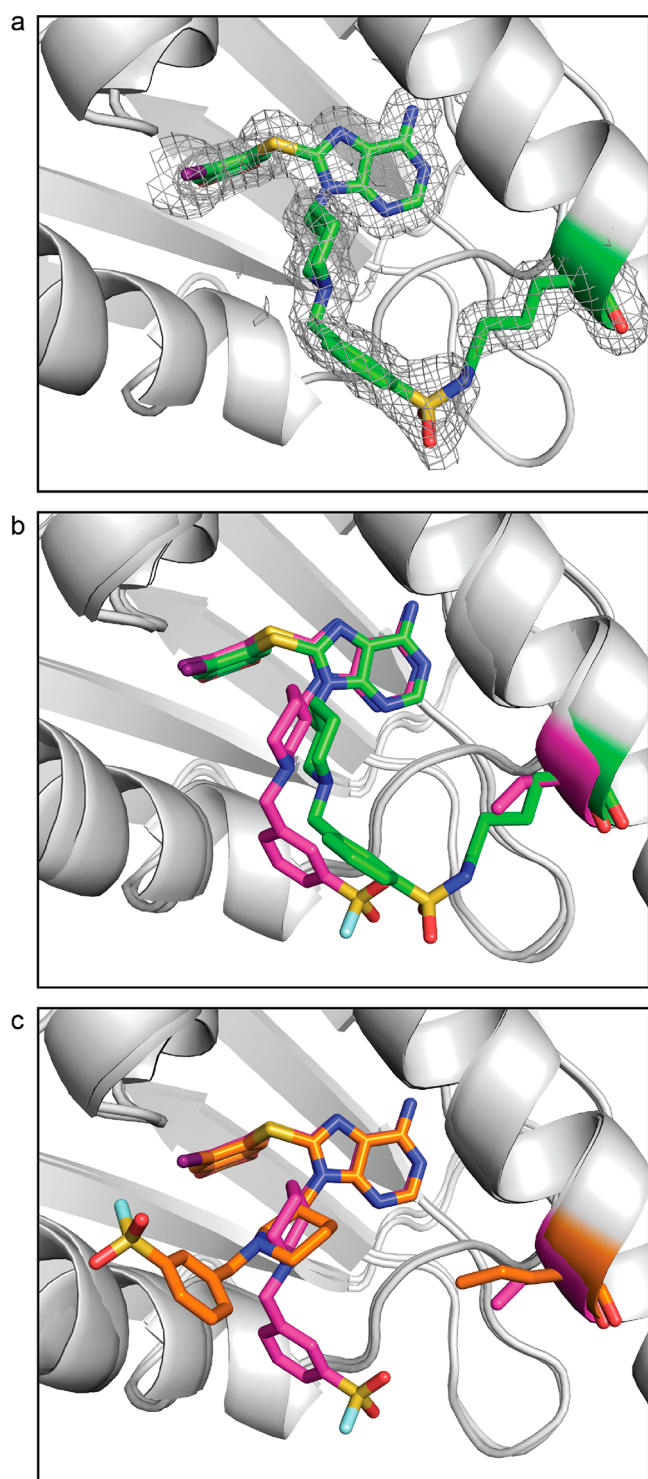


Figure 4. Cocrystal structures of **5** and **6** bound to Hsp90. (a) 1.8-Å resolution crystal structure of **5** covalently bound to Lys58 Hsp90 α NTD. Electron density ($2F_o - F_c$) is shown at a contour level of 1σ . (b) Overlay of (a) with the cocrystal structure of **5** bound reversibly to K58R Hsp90 α NTD. (c) Overlay of cocrystal structures of **5** and **6** reversibly bound to K58R Hsp90 α NTD.

the conformation of the (*S*)-methylpiperidine linker of **5**—in particular, the dihedral between the methylene substituent and the piperidine chiral center—is nearly identical in the covalent and noncovalent complexes (Figure 4b and S5). This arrangement places the electrophilic sulfur atom within ~ 3 Å

of the position it occupies after reacting with Lys58, as observed in the structure of the covalent complex. Strikingly, the (*R*)-methylpiperidine linker in **6** adopts the opposite orientation upon binding to Hsp90. The critical dihedral between the methylene substituent and the piperidine chiral center of **6** ($+164^\circ$) is equal in magnitude but opposite in sign to that of **5** (-177°), such that the arylsulfonyl fluoride in **6** projects away from Lys58Arg and packs against the side chain of Ile110 (Figure 4c and S5). Although this dihedral likely represents a relatively unstrained conformation, we speculate that attractive and repulsive interactions with Hsp90 (and surrounding water molecules) contribute to the conformational preferences observed in the noncovalent structures of both **5** and **6**. We conclude that upon binding to Hsp90, **5** adopts a preferred orientation that places the sulfonyl fluoride within striking distance of Lys58, giving rise to the observed 40-fold enhancement in k_{inact} relative to **6** (Figure 3b).

We next compared the effects of **5** and **6** in Skbr3 cells. Compound **5** exhibited concentration- and time-dependent occupancy of endogenous cellular Hsp90, as revealed by reduced Hsp90 labeling by the competitive clickable probe **2** (Figure 5a and 5b). We inferred from these experiments that cellular Hsp90 was covalently modified by **5** (but not **6**), because (1) the clickable probe **2** was added to cell lysates after extensively washing the cells to remove excess **5** and **6**, and (2) treatment of cells with the enantiomer **6** failed to prevent labeling by probe **2** under these conditions. Continuous treatment of Skbr3 cells with compounds **5**, **6**, and PU-H71 ($3.3 \mu\text{M}$, 6 h) activated the heat shock response (as shown by increased Hsp70 levels) and downregulated known Hsp90 clients, including Her2 (amplified in Skbr3 cells) and phospho-Akt (p-S473), a downstream effector of Her2 signaling (Figure 5c). This is consistent with results from the fluorescence polarization assay showing equipotent reversible binding of both enantiomers **5** and **6** to Hsp90.

To explore the cellular phenotypes resulting from pulsed, covalent inhibition of Hsp90, we treated cells with saturating amounts of **5**, **6**, and PU-H71 ($3.3 \mu\text{M}$) for 90 min, followed by rigorous compound washout. Under these conditions, compound **5** exhibited nearly 100% occupancy immediately after washout, as determined by the absence of subsequent labeling by probe **2** (Figure 6a). As expected, similar treatment with **6** and PU-H71 failed to result in durable Hsp90 occupancy (indicated by $\sim 100\%$ labeling with probe **2**), demonstrating washout of the reversibly bound inhibitors. Surprisingly, levels of the covalent Hsp90-**5** complex decreased over time ($t_{1/2} \sim 12$ h), as shown by the time-dependent increase in Hsp90 labeling with probe **2** (added to cell lysates). Western blotting revealed that levels of total Hsp90 remained constant throughout the washout experiment. Together, these data suggest that **5**-modified Hsp90 is degraded and replaced by newly synthesized, unoccupied Hsp90 (see Figure 7 below). Despite the steady decrease in **5**-modified Hsp90 ($\sim 20\%$ occupancy after 24 h), we observed a sustained heat shock response in cells that were transiently exposed to **5**—but not **6** or PU-H71—as revealed by elevated levels of Hsp70 for at least 24 h post-washout (Figure 6a). Similarly, transient exposure of cells to **5** (and to a lesser extent, **6** and PU-H71) resulted in downregulation of Her2 and phospho-Akt (Figure 6b). However, in contrast to Hsp70 induction, Her2 and phospho-Akt recovered nearly to baseline levels within 24 h post-washout. Hence, the rate at which cells recover from pulsed, covalent inhibition of Hsp90 depends on the cellular

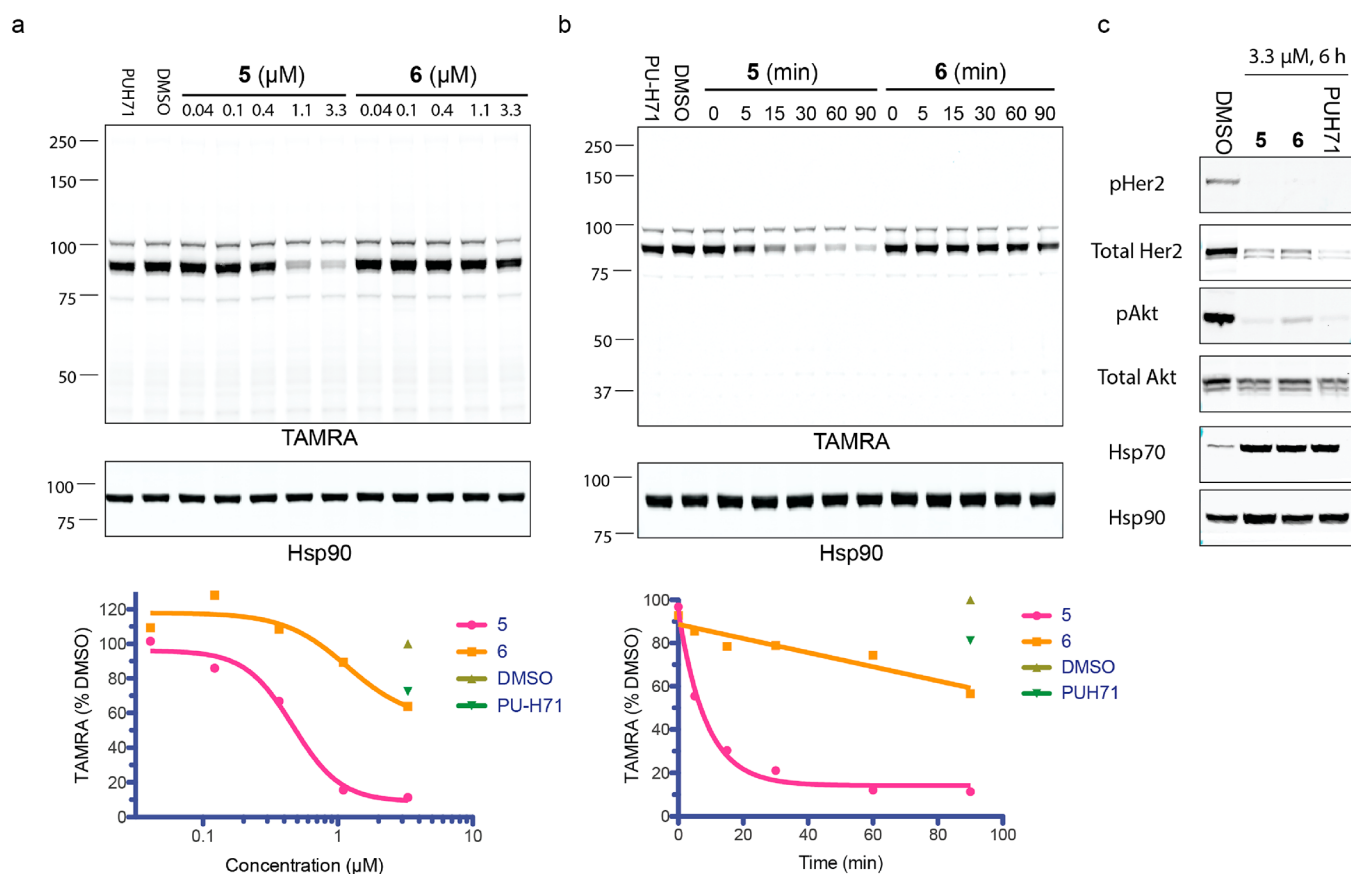


Figure 5. Covalent and noncovalent inhibition of Hsp90 in cells. (a) Skbr3 cells were treated with the indicated concentrations of 5 and 6 for 90 min at 37 °C. After washing the cells, lysates were prepared and treated with probe 2 (3.3 μM, 60 min, 37 °C), followed by click conjugation with TAMRA-azide and in-gel fluorescence analysis. Normalized TAMRA fluorescence intensity (90-kDa band) was plotted. The ~100 kDa band above Hsp90 is nonspecific and was only observed when cell lysates were treated with probe 2 (as opposed to intact cells, see Figure 1f). (b) Skbr3 cells were treated with 5 and 6 (3.3 μM, 37 °C). At the indicated time points, cell lysates were prepared, treated with probe 2, and analyzed as described above. (c). Skbr3 cells were treated with 5, 6, and PU-H71 for 6 h (3.3 μM, 37 °C). Levels of Her2, total Akt, phospho-S473 Akt, Hsp70, and Hsp90 were analyzed by Western blotting.

process, with Her2 resynthesis and activation occurring at a faster rate than Hsp70 downregulation.

The apparent decrease in Hsp90 occupancy by 5—inferred by monitoring the time-dependent increase in Hsp90 labeling by probe 2 (Figure 6a)—could be explained by Hsp90 resynthesis during the washout period, degradation of 5-modified Hsp90, or both. To determine the fate of irreversibly inhibited Hsp90, we treated intact cells with clickable probe 2 (3.3 μM, 90 min) and monitored the covalent Hsp90-2 adduct by in-gel fluorescence after compound washout and rhodamine-azide conjugation in cell lysates. The fluorescent signal from the covalent Hsp90-2 adduct decreased steadily over 24 h, with a half-life of 6–12 h (Figure 7a). Total Hsp90 levels did not change during this time period, likely due to resynthesis of Hsp90 concomitant with degradation of the covalent Hsp90-2 adduct. In contrast to the covalent Hsp90-2 adduct, turnover of unmodified Hsp90 was negligible (Figure 7b), consistent with previous measurements of Hsp90 turnover rates in unperturbed cells ($t_{1/2} > 36$ h).^{28,29} We conclude that covalent modification by compounds 2 and 5 promotes degradation of Hsp90. Further studies are required to elucidate the cellular machinery that mediates this response.

CONCLUSIONS AND PERSPECTIVE

Starting with a reversible, ATP-competitive inhibitor, we designed a series of arylsulfonyl fluorides to irreversibly trap a distal, surface-exposed lysine. Although optimization of irreversible covalent inhibitors (as determined by comparing k_{inact}/K_i values) typically involves maximizing the reversible binding affinity (minimizing K_i), we pursued an alternative strategy. Here, we sought to maximize the rate of covalent bond formation within the noncovalent complex (k_{inact}) by biasing the orientation of the arylsulfonyl fluoride toward the ϵ -amine (proximity-induced rate acceleration). Importantly, we were able to increase k_{inact} without increasing the intrinsic reactivity of the electrophile. Our best covalent Hsp90 inhibitor, arylsulfonyl fluoride 5, employs a chiral, conformationally constrained linker to span the 10-Å distance between the purine noncovalent recognition element and the sulfonyl fluoride. We observed striking enantiodiscrimination at the level of k_{inact} as revealed by biochemical and structural studies. Enantioselectivity was also observed in cells, such that after compound washout, only the (*S*)-enantiomer produced sustained covalent inactivation of endogenous Hsp90. Together, these experiments strongly support our mechanistic interpretation that, upon binding to Hsp90, the (*S*)-methylpiperidine 5 is poised to undergo nucleophilic attack by Lys58, whereas the dominant conformation adopted by

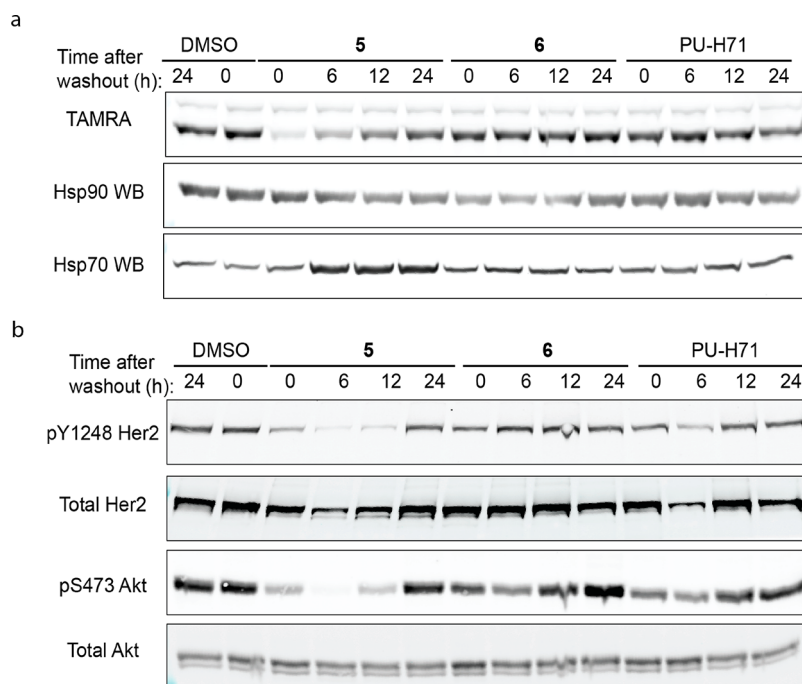


Figure 6. Effects of covalent Hsp90 modification after compound washout. Skbr3 cells were treated with **5**, **6**, or PU-H71 (3.3 μ M, 90 min), followed by extensive compound washout (see Supporting Information for details). At the indicated times post-washout, cell lysates were prepared. (a) Lysates were treated with probe **2**, and Hsp90 occupancy was measured by in-gel fluorescence (TAMRA). In parallel, lysate samples were analyzed by Western blotting for total Hsp90 and Hsp70. (b) Samples described in (a) were analyzed by Western blotting for total and phosphorylated Her2 and Akt.

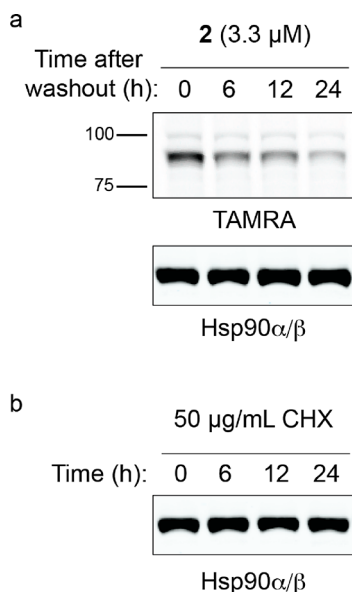


Figure 7. Accelerated turnover of covalently inhibited Hsp90. (a) Skbr3 cells were treated with **2** (3.3 μ M, 90 min) followed by compound washout. At the indicated time points post-washout, cell lysates were prepared. Probe-labeled Hsp90 was visualized by in-gel fluorescence after click conjugation with TAMRA-azide, and total Hsp90 was monitored by Western blotting. (b) Skbr3 cells were treated with 50 μ g/mL cycloheximide. At the indicated time points, Hsp90 levels were determined by Western blotting.

(*R*)-methylpiperidine **6** places the sulfonyl fluoride far away from Lys58.

Recently, the Hamachi group reported a complementary approach for covalently targeting Hsp90, in which an

electrophilic *N*-cyanoethyl acylsulfonamide was employed to acylate Lys58.²⁴ The cyanoethyl acylsulfonamide and arylsulfonyl fluoride Hsp90 inhibitors have similar k_{inact} values, both of which are within the range exhibited by cysteine-targeted covalent drugs.³⁰ A major difference between the two electrophiles concerns the chemical nature of the leaving groups: fluoride vs *N*-cyanoethyl-*N*-arylsulfonamide, with the latter being more lipophilic and sterically demanding. Overall, these studies indicate that arylsulfonyl fluorides and cyanoethyl acylsulfonamides are complementary electrophiles capable of efficiently targeting a surface-exposed lysine.

Our work complements other notable studies in which chiral ligands have been shown to covalently modify their protein targets with high levels of enantioselectivity.^{8,11,31,32} We anticipate that the approach of targeting a surface lysine with an arylsulfonyl fluoride oriented by a chiral, conformationally constrained linker can be applied to myriad targets that lack either a reactive cysteine or a pK_{a} -perturbed lysine within the ligand binding pocket. By analyzing protein-bound small molecules in the Protein Data Bank,¹⁵ we estimate that the vast majority of ligandable sites are within 10 Å of a lysine ϵ -amine. Looking forward, we envision the use of advanced computational methods to aid in the design of chiral, conformationally constrained linkers that maximize the rate of covalent bond formation.

■ ASSOCIATED CONTENT

SI Supporting Information

The Supporting Information is available free of charge at <https://pubs.acs.org/doi/10.1021/jacs.9b09684>.

Supplemental figures and tables, detailed experimental methods including synthesis and characterization of new

compounds, X-ray data collection and refinement statistics (PDF)

AUTHOR INFORMATION

Corresponding Author

Jack Taunton – Department of Cellular and Molecular Pharmacology, University of California, San Francisco, California 94158, United States; orcid.org/0000-0002-9627-5898; Email: jack.taunton@ucsf.edu

Authors

Adolfo Cuesta – Department of Cellular and Molecular Pharmacology, University of California, San Francisco, California 94158, United States; orcid.org/0000-0003-2389-5823

Xiaobo Wan – Department of Cellular and Molecular Pharmacology and Department of Pharmaceutical Chemistry, University of California, San Francisco, California 94158, United States; orcid.org/0000-0003-4288-9074

Alma L. Burlingame – Department of Pharmaceutical Chemistry, University of California, San Francisco, California 94158, United States

Complete contact information is available at:
<https://pubs.acs.org/10.1021/jacs.9b09684>

Notes

The authors declare the following competing financial interest(s): J.T. is a cofounder and shareholder of Global Blood Therapeutics, Principia Biopharma, Kezar Life Sciences, and Cedilla Therapeutics.

ACKNOWLEDGMENTS

Funding for this study was provided by the NCI (NIH NCI F31CA214028, AC) and Pfizer (JT). We thank Jordan Carelli, Sherry Niessen, and John Kath for helpful discussions. Mass spectrometry was supported by the UCSF Program for Breakthrough Biomedical Research (PBBR), the Howard Hughes Medical Institute, and the Adelson Medical Research Foundation (ALB).

REFERENCES

- (1) Singh, J.; Petter, R. C.; Baillie, T. A.; Whitty, A. The Resurgence of Covalent Drugs. *Nat. Rev. Drug Discovery* **2011**, *10*, 307–317.
- (2) Baillie, T. A. Targeted Covalent Inhibitors for Drug Design. *Angew. Chem., Int. Ed.* **2016**, *55* (43), 13408–13421.
- (3) Cohen, M. S.; Zhang, C.; Shokat, K. M.; Taunton, J. Structural Bioinformatics-Based Design of Selective, Irreversible Kinase Inhibitors. *Science* **2005**, *308* (5726), 1318–1321.
- (4) Smith, G. A.; Uchida, K.; Weiss, A.; Taunton, J. Essential Biphasic Role for JAK3 Catalytic Activity in IL-2 Receptor Signaling. *Nat. Chem. Biol.* **2016**, *12*, 373–379.
- (5) Honigberg, L. A.; Smith, A. M.; Sirisawad, M.; Verner, E.; Louny, D.; Chang, B.; Li, S.; Pan, Z.; Thamm, D. H.; Miller, R. A.; et al. The Bruton Tyrosine Kinase Inhibitor PCI-32765 Blocks B-Cell Activation and Is Efficacious in Models of Autoimmune Disease and B-Cell Malignancy. *Proc. Natl. Acad. Sci. U. S. A.* **2010**, *107* (29), 13075–13080.
- (6) Li, D.; Ambrogio, L.; Shimamura, T.; Kubo, S.; Takahashi, M.; Chirieac, L. R.; Padera, R. F.; Shapiro, G. I.; Baum, A.; Himmelsbach, F.; et al. BIBW2992, an Irreversible EGFR/HER2 Inhibitor Highly Effective in Preclinical Lung Cancer Models. *Oncogene* **2008**, *27* (34), 4702–4711.
- (7) Kwiatkowski, N.; Zhang, T.; Rahl, P. B.; Abraham, B. J.; Reddy, J.; Ficarro, S. B.; Dastur, A.; Amzallag, A.; Ramaswamy, S.; Tesar, B.;

et al. Targeting Transcription Regulation in Cancer with a Covalent CDK7 Inhibitor. *Nature* **2014**, *511* (7511), 616–620.

(8) Zhang, T.; Kwiatkowski, N.; Olson, C. M.; Dixon-Clarke, S. E.; Abraham, B. J.; Greifenberg, A. K.; Ficarro, S. B.; Elkins, J. M.; Liang, Y.; Hannett, N. M.; et al. Covalent Targeting of Remote Cysteine Residues to Develop CDK12 and CDK13 Inhibitors. *Nat. Chem. Biol.* **2016**, *12* (10), 876–884.

(9) Strelow, J. M. A Perspective on the Kinetics of Covalent and Irreversible Inhibition. *J. Biomol. Screen.* **2017**, *22* (1), 1–18.

(10) Dalton, S. E.; Dittus, L.; Thomas, D. A.; Convery, M. A.; Nunes, J.; Bush, J. T.; Evans, J. P.; Werner, T.; Bantscheff, M.; Murphy, J. A.; et al. Selectively Targeting the Kinome-Conserved Lysine of PI3K δ as a General Approach to Covalent Kinase Inhibition. *J. Am. Chem. Soc.* **2018**, *140* (3), 932–939.

(11) Cheng, H.; Nair, S. K.; Murray, B. W.; Almaden, C.; Bailey, S.; Baxi, S.; Behenna, D. C.; Cho-Schultz, S.; Dalvie, D.; Dinh, D. M.; et al. Discovery of 1-((3R,4R)-3-[5-Chloro-2-(1-Methyl-1H-Pyrazol-4-Ylamino)-7H-Pyrrolo[2,3-d]Pyrimidin-4-Yloxy)methyl]-4-Methoxy-Pyrrolidin-1-Yl}propanone (PF-06459988), A Potent, WT Sparing, Irreversible Inhibitor of T790M-Containing EGFR Mutants. *J. Med. Chem.* **2016**, *59*, 2005.

(12) Miller, R. M.; Taunton, J. Targeting Protein Kinases with Selective and Semipromiscuous Covalent Inhibitors. *Methods Enzymol.* **2014**, *548*, 93–116.

(13) Liu, Q.; Sabnis, Y.; Zhao, Z.; Zhang, T.; Buhrlage, S. J.; Jones, L. H.; Gray, N. S. Developing Irreversible Inhibitors of the Protein Kinase Cysteinome. *Chem. Biol.* **2013**, *20* (2), 146–159.

(14) Gehringer, M.; Laufer, S. A. Emerging and Re-Emerging Warheads for Targeted Covalent Inhibitors: Applications in Medicinal Chemistry and Chemical Biology. *J. Med. Chem.* **2019**, *62* (12), 5673–5724.

(15) Cuesta, A.; Taunton, J. Lysine-Targeted Inhibitors and Chemoproteomic Probes. *Annu. Rev. Biochem.* **2019**, *88*, 1–17.

(16) Pettinger, J.; Jones, K.; Cheeseman, M. D. Lysine-Targeting Covalent Inhibitors. *Angew. Chem., Int. Ed.* **2017**, *56*, 15200–15209.

(17) Zhao, Q.; Ouyang, X.; Wan, X.; Gajiwala, K. S.; Kath, J. C.; Jones, L. H.; Burlingame, A. L.; Taunton, J. Broad-Spectrum Kinase Profiling in Live Cells with Lysine-Targeted Sulfonyl Fluoride Probes. *J. Am. Chem. Soc.* **2017**, *139* (2), 680–685.

(18) Grimster, N. P.; Connelly, S.; Baranczak, A.; Dong, J.; Krasnova, L. B.; Sharpless, K. B.; Powers, E. T.; Wilson, I. A.; Kelly, J. W. Aromatic Sulfonyl Fluorides Covalently Kinetically Stabilize Transthyretin to Prevent Amyloidogenesis While Affording a Fluorescent Conjugate. *J. Am. Chem. Soc.* **2013**, *135* (15), 5656–5668.

(19) Gushwa, N. N.; Kang, S.; Chen, J.; Taunton, J. Selective Targeting of Distinct Active Site Nucleophiles by Irreversible SRC-Family Kinase Inhibitors. *J. Am. Chem. Soc.* **2012**, *134* (50), 20214–20217.

(20) Liu, R.; Yue, Z.; Tsai, C. C.; Shen, J. Assessing Lysine and Cysteine Reactivities for Designing Targeted Covalent Kinase Inhibitors. *J. Am. Chem. Soc.* **2019**, *141* (16), 6553–6560.

(21) Baggio, C.; Gambini, L.; Udolpholku, P.; Salem, A.; Aronson, A.; Dona, A.; Troadec, E.; Pichiorri, F.; Pellicchia, M. Design of Potent Pan-IAP and Lys-Covalent XIAP Selective Inhibitors Using a Thermodynamics Driven Approach. *J. Med. Chem.* **2018**, *61*, 6350.

(22) Gambini, L.; Baggio, C.; Udolpholku, P.; Jossart, J.; Salem, A. F.; Perry, J. J. P.; Pellicchia, M. Covalent Inhibitors of Protein-Protein Interactions Targeting Lysine, Tyrosine, or Histidine Residues. *J. Med. Chem.* **2019**, *62*, S616.

(23) Taipale, M.; Jarosz, D. F.; Lindquist, S. HSP90 at the Hub of Protein Homeostasis: Emerging Mechanistic Insights. *Nat. Rev. Mol. Cell Biol.* **2010**, *11*, 515–528.

(24) Tamura, T.; Ueda, T.; Goto, T.; Tsukidate, T.; Shapira, Y.; Nishikawa, Y.; Fujisawa, A.; Hamachi, I. Rapid Labelling and Covalent Inhibition of Intracellular Native Proteins Using Ligand-Directed N-Acyl-N-Alkyl Sulfonamide. *Nat. Commun.* **2018**, *9* (1), 1–12.

(25) Immormino, R. M.; Kang, Y.; Chiosis, G.; Gewirth, D. T. Structural and Quantum Chemical Studies of 8-Aryl-Sulfanyl Adenine Class Hsp90 Inhibitors. *J. Med. Chem.* **2006**, *49* (16), 4953–4960.

(26) Taldone, T.; Patel, P. D.; Patel, M.; Patel, H. J.; Evans, C. E.; Rodina, A.; Ochiana, S.; Shah, S. K.; Uddin, M.; Gewirth, D.; et al. Experimental and Structural Testing Module to Analyze Paralogue-Specificity and Affinity in the Hsp90 Inhibitors Series. *J. Med. Chem.* **2013**, *56* (17), 6803–6818.

(27) Kim, J.; Felts, S.; Llauger, L.; He, H.; Huezo, H.; Rosen, N.; Chiosis, G. Development of a Fluorescence Polarization Assay for the Molecular Chaperone Hsp90. *J. Biomol. Screening* **2004**, *9* (5), 375–381.

(28) Welle, K. A.; Zhang, T.; Hryhorenko, J. R.; Shen, S.; Qu, J.; Ghaemmaghami, S. Time-Resolved Analysis of Proteome Dynamics by Tandem Mass Tags and Stable Isotope Labeling in Cell Culture (TMT-SILAC) Hyperplexing. *Mol. Cell. Proteomics* **2016**, *15* (12), 3551–3563.

(29) Zecha, J.; Meng, C.; Zolg, D. P.; Samaras, P.; Wilhelm, M.; Kuster, B. Peptide Level Turnover Measurements Enable the Study of Proteome Dynamics. *Mol. Cell. Proteomics* **2018**, *17* (5), 974–992.

(30) Schwartz, P. a; Kuzmic, P.; Solowiej, J.; Bergqvist, S.; Bolanos, B.; Almaden, C.; Nagata, A.; Ryan, K.; Feng, J.; Dalvie, D.; et al. Covalent EGFR Inhibitor Analysis Reveals Importance of Reversible Interactions to Potency and Mechanisms of Drug Resistance. *Proc. Natl. Acad. Sci. U. S. A.* **2014**, *111* (1), 173–178.

(31) Wang, Y.; Dix, M. M.; Bianco, G.; Remsberg, J. R.; Lee, H. Y.; Kalocsay, M.; Gygi, S. P.; Forli, S.; Vite, G.; Lawrence, R. M.; et al. Expedited Mapping of the Ligandable Proteome Using Fully Functionalized Enantiomeric Probe Pairs. *Nat. Chem.* **2019**, *11*, 1113–1123.

(32) Fowler, J. S.; MacGregor, R. R.; Wolf, A. P.; Arnett, C. D.; Dewey, S. L.; Schlyer, D.; Christman, D.; Logan, J.; Smith, M.; Sachs, H.; et al. Mapping Human Brain Monoamine Oxidase A and B with ¹¹C-Labeled Suicide Inactivators and PET. *Science* **1987**, *235* (4787), 481–485.

■ NOTE ADDED AFTER ASAP PUBLICATION

This paper was published on February 3, 2020. Panel c of Figure 1 has been updated. The revised version re-posted on February 6, 2020.